

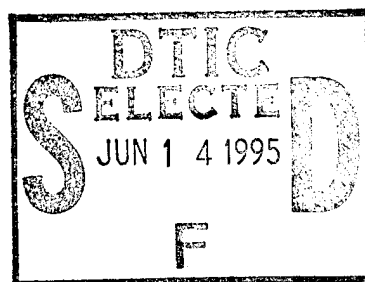
PL-TR-93-2135

SHARC, A COMPREHENSIVE NON-EQUILIBRIUM INFRARED RADIATION MODEL FOR THE UPPER ATMOSPHERE

**R. L. Sundberg
J. W. Duff
L. S. Bernstein
J. H. Gruninger**

**M. W. Matthew
A. Berk
D. C. Robertson
S. M. Adler-Golden**

**Spectral Sciences, Inc.
99 South Bedford Street, #7
Burlington, MA 01803-5169**



21 June 1993

Scientific Report No. 3

APPROVED FOR PUBLIC RELEASE; DISTRIBUTION UNLIMITED

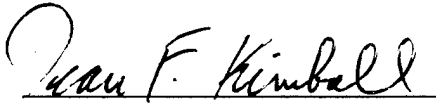


**PHILLIPS LABORATORY
Directorate of Geophysics
AIR FORCE MATERIEL COMMAND
HANSCOM AIR FORCE BASE, MA 01731-3010**

DTIC QUALITY INSPECTED 3

19950612 075

"This technical report has been reviewed and is approved for publication."



DEAN F. KIMBALL
Contract Manager
Simulation Branch



WILLIAM A. M. BLUMBERG, Chief
Simulation Branch
Optical Environment Division



ROGER A. VAN TASSEL, Director
Optical Environment Division

This report has been reviewed by the ESC Public Affairs Office (PA) and is releasable to the National Technical Information Service (NTIS).

Qualified requestors may obtain additional copies from the Defense Technical Information Center (DTIC). All Others should apply to the National Technical Information Service (NTIS).

If your address has changed, if you wish to be removed from the mailing list, or if the addressee is no longer employed by your organization, please notify PL/IM, 29 Randolph Road, Hanscom AFB, MA 01731-3010. This will assist us in maintaining a current mailing list.

Do not return copies of this report unless contractual obligations or notices on a specific document require that it be returned.

| REPORT DOCUMENTATION PAGE | | | Form Approved OMB No. 0704-0188 | |
|--|---|--|------------------------------------|--|
| Public reporting burden for this collection of information is estimated to average 1 hour per response, including the time for reviewing instructions, searching existing data sources, gathering and maintaining the data needed, and completing and reviewing the collection of information. Send comments regarding this burden estimate or any other aspect of this collection of information, including suggestions for reducing this burden, to Washington Headquarters Services, Directorate for Information Operations and Reports, 1215 Jefferson Davis Highway, Suite 1204, Arlington, VA 22202-4302, and to the Office of Management and Budget, Paperwork Reduction Project (0704-0188), Washington, DC 20503. | | | | |
| 1. AGENCY USE ONLY (Leave blank) | 2. REPORT DATE 21 June 1993 | 3. REPORT TYPE AND DATES COVERED Scientific #3 | | |
| 4. TITLE AND SUBTITLE SHARC, A Comprehensive Non-Equilibrium Infrared Radiation Model for the Upper Atmosphere | | 5. FUNDING NUMBERS C - F19628-91-C-0083 PE - 63215C PR - S321 TA - 13 WU - AA | | |
| 6. AUTHOR(S) R. L. Sundberg, J. W. Duff, L. S. Bernstein, J. H. Gruninger, M. W. Matthew, A. Berk, D. C. Robertson, and S. M. Adler-Golden | | | | |
| 7. PERFORMING ORGANIZATION NAME(S) AND ADDRESS(ES) Spectral Sciences, Inc. 99 South Bedford Street, #7 Burlington, MA 01803-5169 | | 8. PERFORMING ORGANIZATION REPORT NUMBER SSI-TR-228 | | |
| 9. SPONSORING, MONITORING AGENCY NAME(S) AND ADDRESS(ES) Phillips Laboratory 29 Randolph Road Hanscom AFB, MA 01731-3010 Contract Manager: Dean Kimball/GPOS | | 10. SPONSORING, MONITORING AGENCY REPORT NUMBER PL-TR-93- 2135 | | |
| 11. SUPPLEMENTARY NOTES | | | | |
| 12. DISTRIBUTION AVAILABILITY STATEMENT Approved for Public Release; Distribution Unlimited | | 13. DISTRIBUTION CODE | | |
| 13. ABSTRACT (Maximum 200 words) A new, first-principles computer model, SHARC, has been developed by the Air Force for the rapid and accurate calculation of non-LTE upper atmospheric infrared radiance and transmittance spectra with a resolution of better than 1 cm^{-1} . Comprehensive coverage of the $2 \text{ }\mu\text{m}$ to $40 \text{ }\mu\text{m}$ (250 cm^{-1} to $5,000 \text{ cm}^{-1}$) wavelength region is provided for arbitrary lines of sight in the 50 - 300 km altitude range, accounting for the detailed production, loss, and energy transfer processes among the molecular vibrational states. Auroral production and excitation of CO_2 , NO , and NO^+ are included in addition to quiescent atmospheric processes. Calculated vibrational temperatures are found to be similar to results from other non-LTE codes, and SHARC's equivalent-width spectral algorithm provides very good agreement with much more time-consuming "exact" line-by-line methods. | | | | |
| 14. SUBJECT TERMS infrared radiance atmosphere aurora spectrum | | | 15. NUMBER OF PAGES 32 | |
| | | | 16. PRICE CODE | |
| 17. SECURITY CLASSIFICATION OF REPORT UNCLASSIFIED | 18. SECURITY CLASSIFICATION OF THIS PAGE UNCLASSIFIED | 19. SECURITY CLASSIFICATION OF ABSTRACT UNCLASSIFIED | 20. LIMITATION OF ABSTRACT SAR | |

TABLE OF CONTENTS

| <u>Section</u> | <u>Page</u> |
|--|-------------|
| 1. INTRODUCTION | 1 |
| 2. CODE DESCRIPTION | 3 |
| 2.1 Quiescent Chemical Kinetics | 4 |
| 2.2 Radiative Excitation from Atmospheric Layers | 6 |
| 2.3 Sample Results for CO ₂ | 7 |
| 2.4 Auroral Kinetics Model | 8 |
| 2.4.1 Secondary Electron Kinetics | 9 |
| 2.4.2 Formation of NO and NO ⁺ | 9 |
| 2.4.3 Vibrational Excitation of CO ₂ and N ₂ | 10 |
| 2.4.4 Radiative Transfer | 11 |
| 2.5 Line-of-Sight Spectral Radiance Model | 13 |
| 2.5.1 Calculation for a Single Line | 13 |
| 2.5.2 Calculation for Multiple Lines | 15 |
| 2.5.3 Illustrative Calculations | 16 |
| 3. DATA COMPARISONS | 19 |
| 4. CONCLUSIONS | 23 |
| 5. ACKNOWLEDGEMENTS | 24 |
| 6. REFERENCES | 25 |

LIST OF ILLUSTRATIONS

| <u>Figure</u> | <u>Page</u> |
|---|-------------|
| 1 SHARC Module Structure and Computational Sequence | 3 |
| 2 Vibrational Temperature Profiles for Selected CO ₂ States | 8 |
| 3 Steady-State Secondary Electron Distribution at an Altitude of 100 km for a Class III ⁺ Aurora | 10 |
| 4 Prediction of the N ₂ (v) Production Efficiency for Several Mechanisms | 11 |
| 5 Comparison of CO ₂ (ν ₃) Populations with Different Treatments of Atmospheric Radiative Excitation | 12 |

| | | |
|--|---|---|
| <div style="position: relative; height: 100px;"> <div style="position: absolute; top: 0; right: 0; width: 100%; height: 100%; border: 1px solid black; opacity: 0.5;"></div> <div style="position: absolute; bottom: 10px; left: 10px; font-size: 2em; font-family: cursive;">A-1</div> </div> | <div style="position: relative; height: 100px;"> <div style="position: absolute; top: 0; right: 0; width: 100%; height: 100%; border: 1px solid black; opacity: 0.5;"></div> </div> | <div style="position: relative; height: 100px;"> <div style="position: absolute; top: 0; right: 0; width: 100%; height: 100%; border: 1px solid black; opacity: 0.5;"></div> </div> |
| Dist | and/or special | Codes |

LIST OF ILLUSTRATIONS (CONTINUED)

| <u>Figure</u> | <u>Page</u> |
|---------------|--|
| 6 | Comparison of SHARC and FASCOD3 Calculations of CO ₂ Radiance for a 50 km Limb View 18 |
| 7 | Comparison of SHARC Calculation and Observation of Quiescent Nighttime Emission in a Near-Limb View from an Altitude of 78 km 20 |
| 8 | CO ₂ 4.3 μ m Band Limb Radiance Measured in the SPIRE Rocket Experiment and Predicted by SHARC for Different Solar Zenith Angles Near the Dawn Terminator 21 |
| 9 | Calculated and Observed NO Spectrum for a 90 km Zenith View During a Class II Aurora 22 |

LIST OF TABLES

| <u>Table</u> | <u>Page</u> |
|--------------|---|
| 1 | Quiescent Radiating Species in SHARC 5 |
| 2 | Calculated Radiances for Strong Line (Q10) of CO ₂ ν_2 17 |
| 3 | Calculated Radiances for Weak Line (R56) of CO ₂ ν_2 17 |

1. INTRODUCTION

The calculation of infrared (IR) radiance and transmittance spectra is an important ingredient in many areas of atmospheric science. These include modeling the atmospheric energy budget for global climate change predictions, analyzing data from remote sounding experiments, and understanding molecular excitation and production processes. Typically, a large number of calculations are required that span an extensive spectral/spatial domain. For the upper atmosphere, non-local thermodynamic equilibrium (non-LTE) effects must also be treated.

Available computer codes for atmospheric IR radiation that have gained wide use include several developed and maintained by the US Air Force. LOWTRAN¹ and MODTRAN² are rapid, LTE codes for low- to moderate-resolution spectra. FASCODE³ is a high-resolution, line-by-line code that can be used in both LTE and non-LTE applications; however, the non-LTE molecular state populations must be externally generated. Until recently, a rapid and unified standard code for first-principles calculations of non-LTE atmospheric background radiation has been lacking.

This report briefly describes technical aspects of a new Air Force non-LTE code for atmospheric IR spectra that has sufficient accuracy, speed, and resolution (0.5 cm^{-1}) for a wide range of applications and provides a comprehensive treatment of all important molecular species. SHARC, the Strategic High-altitude Atmospheric Radiation Code,⁴⁻⁶ calculates emission and transmittance spectra in the $2\text{-}40\text{ }\mu\text{m}$ region for arbitrary line-of-sight (LOS) paths between 50 and 300 km. It incorporates the IR bands of NO, CO₂, O₃, H₂O, OH, CO, and CH₄ found in the quiescent atmosphere, including minor isotopic bands of CO₂ and H₂O. It also accounts for auroral production and excitation of CO₂, NO, and NO⁺ caused by the flux of energetic solar electrons. Proton fluxes are not presently modeled but could be accommodated in a similar manner.

To account for non-LTE effects, molecular vibrational state populations are calculated from first principles. As in other non-LTE atmospheric models (e.g., Wintersteiner et al.,⁷ Lopez-Puertas et al.^{8,9}) steady-state kinetics are assumed for the quiescent atmospheric processes of collisional excitation, de-excitation, energy transfer, radiative decay, illumination by the sun, earth and atmosphere, and chemical production. In SHARC, additional production and excitation mechanisms resulting from electron deposition are included using a time-dependent kinetic model. Rotation-translation equilibrium is assumed.

The calculated vibrational state populations are input to a LOS spectral radiance module, which uses a line-by-line (LBL) equivalent width formalism. If desired, the populations may be fed to an external spectral model such as FASCODE, which can provide better resolution and accuracy, although at a considerable time penalty. Our own comparisons indicate nearly a two-order-of-magnitude improvement in speed using the equivalent width approach compared to the standard LBL grid method, with typical radiance errors of less than 10%.

SHARC is written in FORTRAN-77 and has a modular structure to facilitate troubleshooting, modifications, and additions to the kinetic and spectroscopic databases and molecular species. A menu-driven user interface is included. In addition to its usefulness for strategic background calculations, SHARC should be valuable for atmospheric remote sounding and energy transport applications. The code is available for use by the scientific community, and may be obtained from the Phillips Laboratory/GPOS (formerly the Air Force Geophysics Laboratory).¹⁰

2. CODE DESCRIPTION

The schematic in Figure 1 illustrates SHARC's module structure and overall calculational sequence. The input module queries the user for parameters needed to define the calculation. Atmospheric temperature and species density profiles are specified via an external file. Profiles are required for the IR-active species (NO, CO₂, H₂O, O₃, CO, OH, and CH₄), the major atmospheric species to which they are collisionally coupled (N₂, O₂, O), and atomic hydrogen, whose reaction with O₃ provides the main source of OH(v). Other input parameters include the LOS specifications and, if desired, the coordinates of a localized auroral region through which the LOS may pass.

Excited vibrational state populations are calculated in the chemical kinetics and radiative transfer modules and are saved in an output file for later use. For the quiescent atmosphere, steady-state conditions are assumed. If auroral excitation is specified, a time-dependent chemical model calculates the additional production of NO and NO⁺ arising from interactions of auroral electrons. To generate the desired LOS spectrum, the vibrational state populations are fed to the spectral radiance module, which outputs radiance and transmittance spectra and in-band intensities.

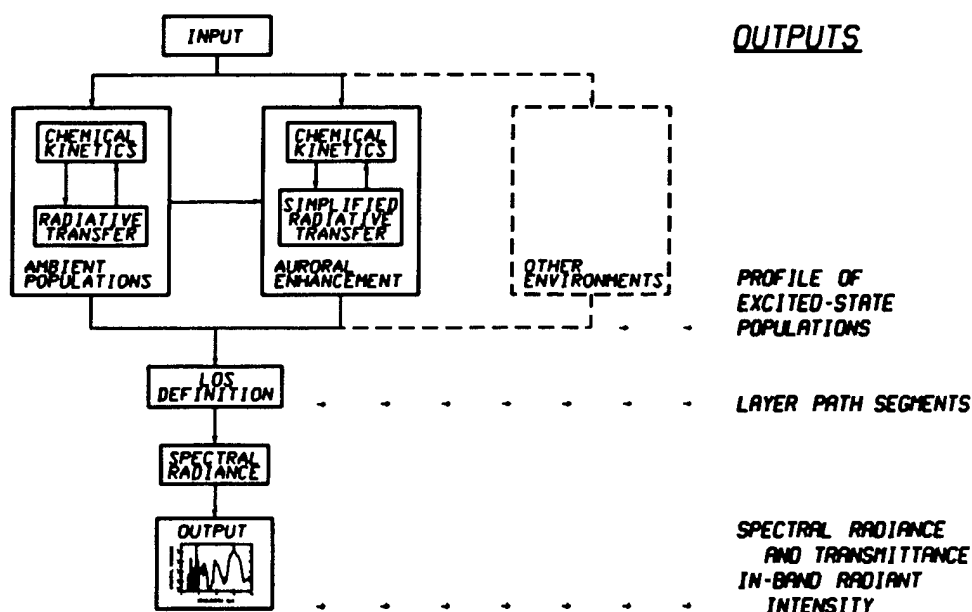


Figure 1. SHARC Module Structure and Calculational Sequence.

Condensed descriptions of the calculations are given below. Detailed descriptions of SHARC may be found in several technical reports.^{4-6,11,12} Code upgrades in progress are indicated by the dotted lines in Figure 1. These upgrades include provisions for LOS's through multiple, distinct atmospheric regions, for use in modeling terminator, tidal, gravity wave, or other atmospheric inhomogeneities.

2.1 Quiescent Chemical Kinetics

The quiescent chemical kinetics are handled primarily through separate reaction sets for each IR-active molecule; the reaction sets can be solved selectively for the specific molecules under investigation. The reaction database files contain the list of vibrational states for each molecule, the chemical equations written in symbolic form, and the rate constant expressions. The equations include chemical formation of excited vibrational states, collisional deactivation and excitation (satisfying detailed balance), spontaneous emission, and the radiative excitation processes associated with absorption of radiation from the sun and from the atmosphere. The size of the database is indicated in Table 1. The atmosphere is assumed to be horizontally uniform and is divided into altitude layers that are typically 2 km to 10 km in height.

The SHARC CHEMKIN module, taken from the Sandia CHEMKIN general-purpose chemical kinetics code,¹³ reads the reaction files and sets up the time-dependent differential rate equations. Each quiescent vibrational state number density $[M^*]$ in each atmospheric layer is obtained from the solution to the steady-state equation

$$0 = d[M^*]/dt = -A[M^*] + \sum_k S_k - \sum_k Q_k[M^*] + r_s + r_e + r_a, \quad (1)$$

where A is the total spontaneous emission rate, the S_k are the source terms for production by collisional processes, and the Q_k are the collisional quenching rates. r_s , r_e , and r_a are the production rates due to radiation from the sun, earth (i.e., from below the 50 km altitude boundary of SHARC), and atmosphere (above 50 km); they depend implicitly on the densities of the lower-energy states of species M . Equation (1) is solved for $[M^*]$ with the constraint that the total number density for the molecule equals that specified in the atmosphere input file.

Table 1. Quiescent Radiating Species in SHARC.

| Molecule | Isotope ^a | States | Reactions | Bands |
|------------------|----------------------|--------|-----------|-------|
| CO ₂ | 626 | 28 | 217 | 34 |
| CO ₂ | 636 | 28 | 217 | 34 |
| CO ₂ | 628 | 28 | 217 | 34 |
| H ₂ O | 161 | 8 | 32 | 14 |
| H ₂ O | 181 | 8 | 32 | 8 |
| H ₂ O | 171 | 8 | 32 | 7 |
| H ₂ O | 162 | 8 | 32 | 7 |
| O ₃ | 666 | 30 | 176 | 45 |
| NO | 46 | 3 | 5 | 3 |
| CO | 26 | 3 | 9 | 3 |
| OH | 61 | 10 | 32 | 24 |
| CH ₄ | 21111 | 12 | 52 | 13 |

^a 1 = ¹H, 2 = ²H or ¹²C, 3 = ¹³C, 4 = ¹⁴N, 6 = ¹⁶O, 7 = ¹⁷O, 8 = ¹⁸O

While most of the excitation and de-excitation processes involve only a single vibrationally excited molecule, leading to uncoupled, linear equations, the species CO₂(v), H₂O(v) and OH(v) are indirectly coupled to each other via resonant energy transfer processes involving N₂(v=1), as discussed by Kumer and co-workers.¹⁴⁻¹⁶ The steady-state equations for these species are linearized by equating the ground vibrational state number densities with the total number densities, and are solved for the N₂(v=1) population. The result is then inserted into the uncoupled Eqs. (1) from which refined excited state populations are calculated. For energy transfer processes involving O₂(v=1),⁹ O₂ is assumed to remain in LTE.

The collisional rate constants were obtained from the recent literature and from Taylor's review¹⁷ of measurements prior to 1974. Further details are given in a technical report.¹² The solar excitation rates k_s are derived from transmittance calculations using

either MODTRAN² or the LOS radiance model discussed in Subsection 2.5. The earthshine rates k_e are expressed in terms of an effective blackbody temperature corresponding to the altitude where the vibrational band becomes optically thick in a nadir view.

The calculation of the excitation rate r_a due to atmospheric emission originating within the 50-300 km altitude range is considerably more complicated than for r_s and r_e , and is performed in a subroutine dubbed NEMESIS, briefly described below.

2.2 Radiative Excitation from Atmospheric Layers

The effect of the atmospheric excitation term r_a is to enhance the excited state number density within each atmospheric layer by an amount

$$\frac{r_a}{A+q} = [M^*] - [M^*]_0 \quad (2)$$

Here q is the total quenching rate and $[M^*]_0$ is the steady-state solution with r_a set to zero, as obtained from an initial CHEMKIN run. Re-excitation due to transfer from $N_2(v=1)$ is incorporated as a reduction in q rather than as a separate source term in Equation (1).

The excited-state enhancement, and hence r_a , may be evaluated following the treatment of Kumer and co-workers.^{14,15} For a given vibrational band and atmospheric layer i we may write

$$[M^*_i] = [M^*_i]_0 + \alpha_i \omega_i \sum_j P_{ji} \omega_j [M^*_j] \quad (3)$$

where α_i is the probability for absorption of a photon entering the layer, P_{ji} is the probability that a photon emitted from layer j will be absorbed in layer i , and ω_i is the branching ratio for re-emission,

$$\omega_i = \frac{A^*}{A+q_i} \quad (4)$$

where A^* is the Einstein coefficient for emission in the given band.

For a calculated probability matrix (P) and set of α_i , the set of Equations (3) for all layers may be solved simultaneously. A physically instructive solution is provided by repeated substitution into Equation (3) of the corresponding equation for the layers j . After collecting factors the result is the infinite series

$$[M^*]_i = [M^*]_{i0} + \alpha_i \omega_i \sum_j (P_{ji}^{(1)} + P_{ji}^{(2)} + \dots) \omega_j [M^*]_{j0} \quad (5)$$

Here the $(P)^{(k)}$ matrices represent probabilities for k-th order photon scattering; $(P)^{(1)} = (P)$. Except in the case of the $\text{CO}_2 \nu_3$ band, which is strongly trapped, the series converges in a small number of terms.

Both (P) and the α_i depend on the lower vibrational state populations. Therefore, the overall solution proceeds in stages for successively higher-energy states. The first CHEMKIN run (with all $r_a = 0$) defines the ground state populations $[M_i]$ and the initial excited state populations $[M^*]_{i0}$ for transitions to the ground state. The results are used in the NEMESIS subroutine to evaluate (P) and α_i and compute the radiative excitation rates r_a for those transitions. CHEMKIN is then rerun including the r_a to generate the corresponding populations for the next set of vibrational transitions. The CHEMKIN/NEMESIS sequence is repeated until solutions for the highest-energy states are obtained.

The major calculational effort is in computing the elements of the layer-layer excitation probability matrix (P) . This involves a multidimensional integral over the location, direction, vibration-rotation line, frequency location within the line, and propagation distance of the radiation. The integral is evaluated with the aid of Monte Carlo sampling using trial "photons". The calculation assumes semi-infinite plane-parallel geometry and uses the exact temperature- and pressure-dependent Voigt lineshape. A more detailed description of the calculation is given elsewhere.¹¹

2.3 Sample Results for CO_2

Sample SHARC results for vibrational states excited by both atmospheric and solar radiation appear in Figure 2, which displays vibrational temperatures for selected states of CO_2 at a solar zenith angle of 82° . The states are labeled using the HITRAN convention;¹⁸ only the main isotopes are shown. This calculation was performed to simulate emissions observed near the dawn terminator during the SPIRE rocket experiment.¹⁹ The species number density and temperature profiles were obtained using the MSISE-90 model²⁰ and an altitude-dependent CO_2 mixing ratio representative of rocket and satellite observations.^{7,21} Up to 10,000 Monte Carlo "photons" per band were used in the NEMESIS runs, which was sufficient to essentially converge the vibrational temperatures.

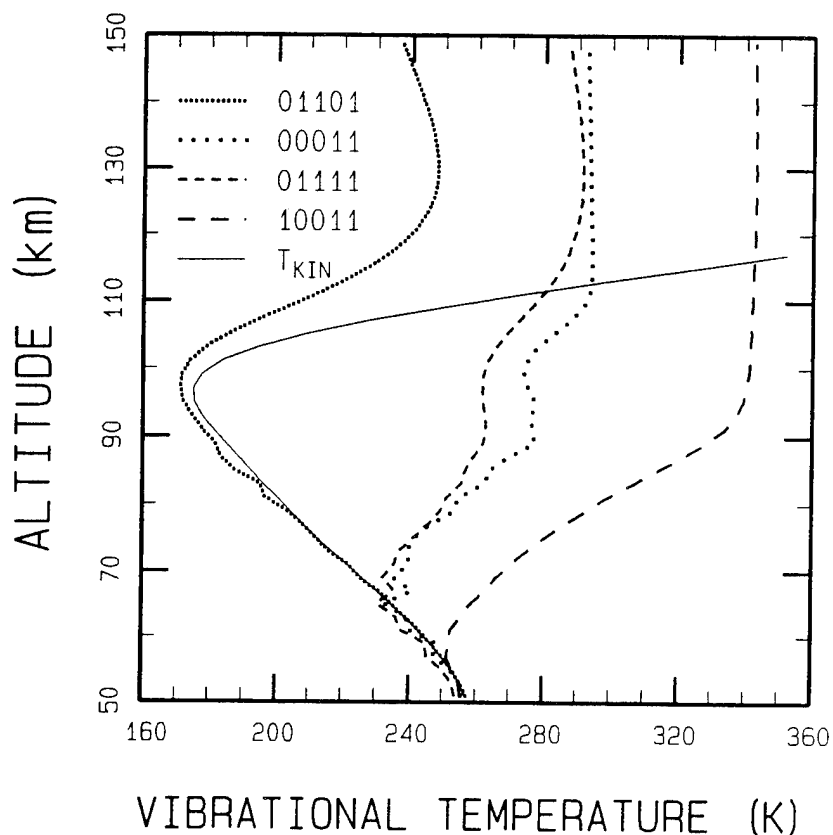


Figure 2. Vibrational Temperature Profiles for Selected CO₂ States.

As seen in Figure 2, the ν_3 -excited states (00011), (01111), and (10011) depart from LTE around 60-70 km altitude. Very similar vibrational temperatures have been reported by Wintersteiner et al.²² using the Air Force Phillips Laboratory "RAD" algorithm. The (01101) (ν_2) state has been treated theoretically in recent studies by Lopez-Puertas et al.²³ and Wintersteiner et al.⁷ The SHARC calculation for Figure 2 used the value $3 \times 10^{-13} \sqrt{T}$ cm³/molec/s for the rate constant for collisional excitation of (01101) by O atoms, consistent with those studies, and consequently generates a similar vibrational temperature profile, which remains close to LTE up to 100 km.

2.4 Auroral Kinetics Model

The SHARC auroral kinetics model calculates the enhancements of CO₂, NO, and NO⁺ radiation resulting from energy deposited in the upper atmosphere by solar electrons.

Approximately 600 time- and energy-dependent rate equations are used to calculate the secondary electron distribution and the subsequent reactive and energy-transfer processes. The energy deposition model for the primary electrons is based on work by Grün, Rees and Strickland²⁴⁻²⁶ as implemented in the Air Force Phillips Laboratory code AARC.²⁷ The chemical reactions and energy transfer processes are described in detail in References 12 and 27. The integration of the time-dependent differential equations is accomplished using the Gear algorithm supplied with the Sandia CHEMKIN code.¹³

The use of time-dependent kinetics results in a significant improvement over the steady-state treatment used in AARC. For example, according to SHARC the NO($v=1$) production efficiency per ion pair increases with time during the aurora as the result of collisional excitation of the increasing concentration of ground state NO.

2.4.1 Secondary Electron Kinetics

Secondary electrons are formed via collisional excitation of N₂, O₂, or O, and undergo further collisions with atmospheric species, resulting in relaxation of the electrons and production of ionic and electronically excited molecular states. The features and altitude dependence of secondary electron distributions in the atmosphere have been discussed in detail elsewhere.²⁸ In SHARC, the secondary electrons are divided into fourteen energy bins. A distribution predicted for a Class III⁺ aurora is shown in Figure 3. The strong dip around 3 eV is due to vibrational excitation of N₂, which in turn provides the energy source for the delayed CO₂ ν_3 auroral emissions.

2.4.2 Formation of NO and NO⁺

When the electrons interact with ambient upper atmospheric species, ionization generates odd nitrogen in the form of N(²P), N(²D), and the ground state, N(⁴S). The production mechanisms in SHARC are direct dissociation of N₂ by the primary electrons, recombination of ions (e.g., NO⁺) with secondary electrons, and charge transfer reactions of the primary ionic products. Collisions between nitrogen atoms and O₂ create NO. The net production rate is highly sensitive to the ratio of N(²D) to N(⁴S) formed, as the NO is formed primarily by reaction with N(²D) and destroyed by reaction with N(⁴S). The vibrationally excited NO is quenched by O and O₂ and also undergoes radiative relaxation.

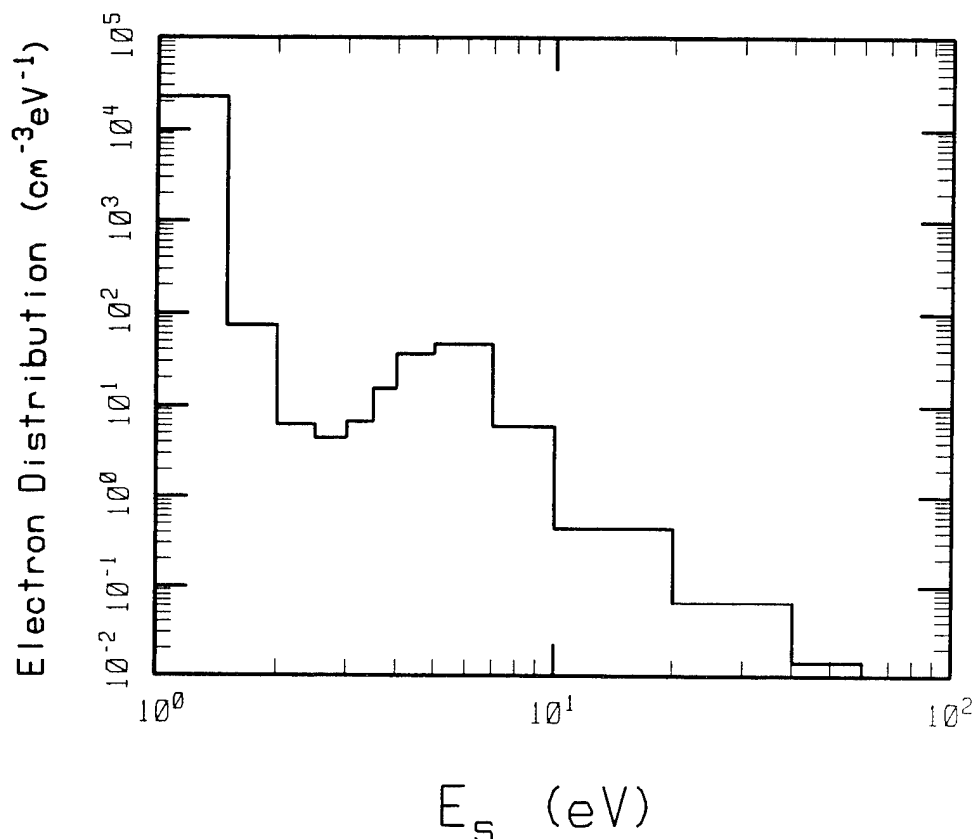


Figure 3. Steady-State Secondary Electron Distribution at an Altitude of 100 km for a Class III⁺ Aurora.

NO^+ is assumed to be formed primarily via the ion-molecule reaction of N^+ with O_2 , which competes with the charge exchange reaction forming O_2^+ . $\text{NO}^+(\nu)$ is quenched by N_2 and by radiative relaxation.

2.4.3 Vibrational Excitation of CO_2 and N_2

$\text{CO}_2(\nu_3)$ is efficiently excited by direct electron impact, which is prompt, and by energy transfer from $\text{N}_2(\nu=1)$, which is delayed. The vibrationally excited N_2 is presumed to arise from the $\text{N}(^4\text{S}) + \text{NO}$ reaction and from the quenching of $\text{O}(^1\text{D})$, and is removed by relaxation with O atoms and transfer to $\text{CO}_2(\nu_3)$. In SHARC, the $\text{N}_2(\nu)$ density is calculated simultaneously with the secondary electron distribution.

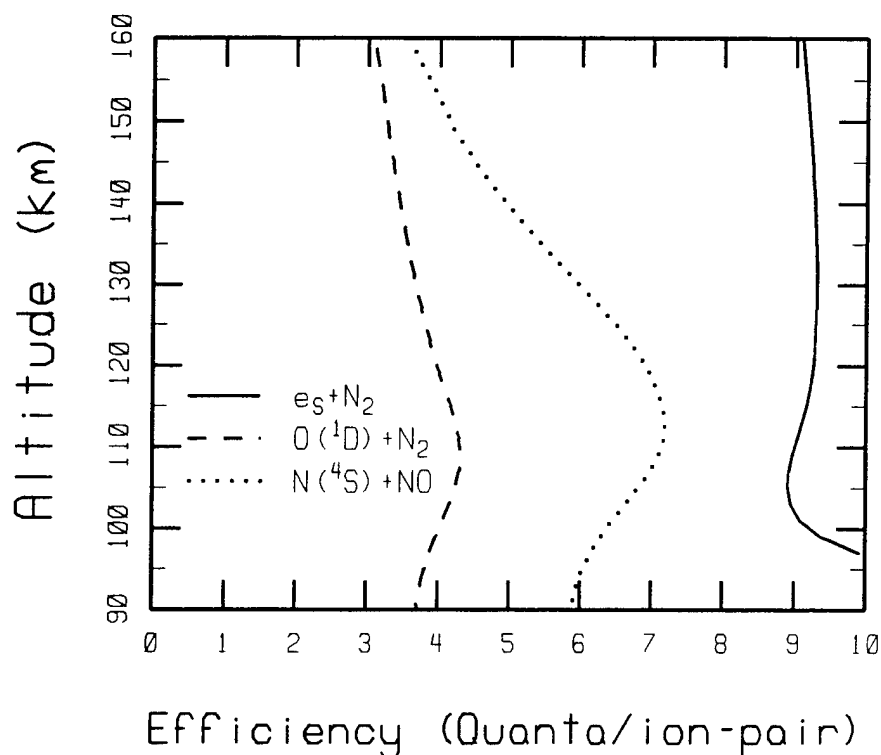


Figure 4. Prediction of the $N_2(v)$ Production Efficiency for Several Mechanisms.

Figure 4 shows the $N_2(v)$ excitation efficiency for a typical calculation. It is seen that direct electronic excitation of N_2 is almost as important as its chemical production, and there is only a slight altitude dependence to the efficiencies.

2.4.4 Radiative Transfer

Emissions from NO and NO^+ are both optically thin and prompt. Therefore, coupling of the radiative transfer and collisional processes is not required, and the solutions to the collisional mechanisms suffice. However, $CO_2(\nu_3)$ emission below 100 km is both optically thick and delayed, so that coupling of the CO_2 time-dependent chemical kinetics to a radiative transfer scheme is required. With the present kinetic scheme, a full treatment would require solving approximately 4000 coupled differential equations, which is impractical. Therefore, a modified escape function approximation (EFA) drawing on the work of Kumer²⁹ is currently adopted.

In Kumer's EFA, it is assumed that photons emitted from a given layer either escape the atmosphere or are re-absorbed within that layer. A comparison between the EFA and a full NEMESIS radiative excitation solution for a quiescent atmosphere is shown in Figure 5. Here "source" labels the $\text{CO}_2(\nu_3)$ density calculated from CHEMKIN alone, while the other curves show the results including radiative excitation enhancement. It is seen that the EFA agrees well with the accurate NEMESIS calculations below 70 km and above 130 km; this simply results from the EFA being correct in the optically thin limit and in the limit of complete photon absorption within the original layer. However, an order-of-magnitude error can occur between those altitudes.

To insure that the correct result is obtained in the limit of negligible auroral excitation, SHARC includes a correction which forces a match to the exact NEMESIS solution for ambient conditions. The correction consist of a time-independent source or sink term added to the differential equation for production of $\text{CO}_2(\nu_3)$, whose magnitude is determined by requiring the auroral production of $\text{CO}_2(\nu_3)$ to be zero at the start of the excitation.

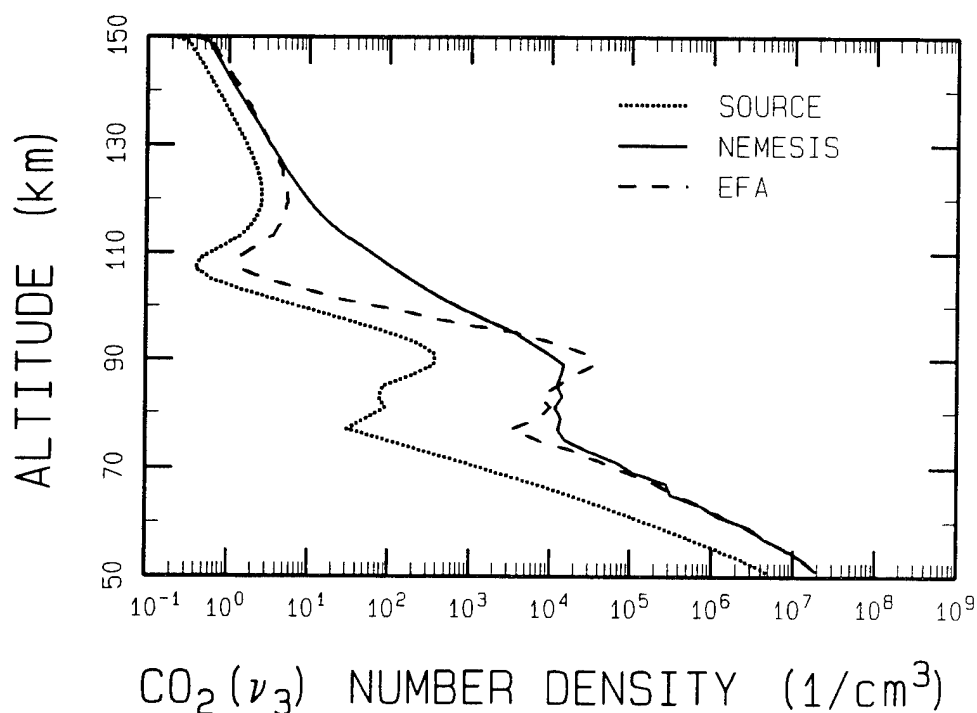


Figure 5. Comparison of $\text{CO}_2(\nu_3)$ Populations with Different Treatments of Atmospheric Radiative Excitation.

2.5 Line-of-Sight Spectral Radiance Model

The LOS spectral radiance is calculated by numerically integrating the radiation transport equation along the LOS path. The approach in SHARC is based on an equivalent-width formulation for single lines. It is around 100 times faster than the usual line-by-line (LBL) grid method, which numerically integrates over the line shape. The spectral resolution of the calculation can be made as high as 0.5 cm^{-1} throughout the 50-300 km altitude range. Above 60 km, the lines are sufficiently narrow and optically thin that the resolution can be increased to 0.1 cm^{-1} .

The inhomogeneous LOS path is represented with a series of homogeneous atmospheric layers, and the equivalent width is calculated using an expression appropriate for Voigt line shapes. The mean line strength and width are derived from the Curtis-Godson approximation.^{30,31} After calculating the equivalent width for each line, the combined equivalent width for all lines within the spectral bin is calculated using an approximate (but typically small) correction for line overlap. Comparison to exact LBL calculations demonstrate that the overall errors in this approach are less than 10% for typical cases.

2.5.1 Calculation for a Single Line

With the atmosphere represented as a series of N homogeneous layers, the equation of LOS radiation transport for a single molecular line is given by³²

$$I = \sum_{i=1}^N R_i (W_{i+1} - W_i) , \quad (6)$$

where the path is from the observer to the beginning of the i th layer, I is the observed radiance, i is the index for each atmospheric layer, R_i is the molecular emission source function (in $\text{W/cm}^2/\text{sr/cm}^{-1}$), and W_i is the equivalent width of the line. The emission source function is given by

$$R = \frac{C_1 \nu^3}{\pi} \frac{\gamma}{1-\gamma} , \quad (7)$$

where C_1 is the first radiation constant and γ is the ratio of upper to lower state populations, defined by

$$\gamma = \frac{g_l}{g_u} \frac{\rho_u}{\rho_l} . \quad (8)$$

The subscript (l or u) denotes the lower or upper state, g is the degeneracy, and ρ is the number density. The states in Equation (7) are defined by their vibrational, rotational and electronic labels, and the number densities in Equation (8) are those calculated from the CHEMKIN and NEMESIS routines. For LTE conditions, $\gamma = \exp(-C_2\nu/T)$, where C_2 is the second radiation constant, and R reduces to the standard Planck blackbody function.

The equivalent width of the line, W , is defined as its integrated absorptance. For the total N -layer path, the transmittance within a spectral interval $\Delta\nu$ containing the line is

$$\tau = 1 - \frac{W_N}{\Delta\nu} \quad (9)$$

in the limit that $\Delta\nu \gg W_N$, where W_N is the total path equivalent width. If $\Delta\nu$ represents the spectral bin width, then in practice it need only be slightly larger than W_N for the transmittance to remain physically valid ($\tau < 1$) and for the radiance I in Equation (6) to be accurate for several-bin-wide averages. Within the altitude range of SHARC, atmospheric linewidths are less than 0.01 cm^{-1} , and equivalent widths remain small enough over the entire spectrum that $\Delta\nu$ can be set as low as 0.5 cm^{-1} .

For Voigt lineshapes, which apply to upper atmospheric conditions, the Rodgers-Williams approximation³³ to the single-line equivalent width provides a reasonable compromise between computational efficiency and accuracy. It is given by

$$W_V^2 = \alpha_D \frac{2}{\ln 2} \left[W_L^2 + W_D^2 - \left(\frac{W_L W_D}{W_W} \right)^2 \right] , \quad (10)$$

where the subscripts V, D, L, and W refer to Voigt, Doppler, Lorentz, and weak-line limits, and $\alpha_D (\text{cm}^{-1})$ is the Doppler linewidth. The equivalent widths are calculated using the approximations³²

$$W_W^2 = \frac{\ln 2}{2} \left[\frac{S_u}{\alpha_D} \right]^2 , \quad (11)$$

$$W_D^2 = \ln(1 + W_W^2) , \quad (12)$$

$$W_L^2 = \frac{[Su]^2}{1 + Su/4\alpha_L} , \quad (13)$$

where α (cm^{-1}) is the line width, S (cm/molecule) is the line strength, and u (molecules/cm^2) is the absorber column density. The errors in the computed W_V are comparable to the 8% peak errors in the approximations for W_D and W_L . These expressions for W_D and W_L are more quickly calculated than the more accurate polynomial series of Rodgers and Williams.

Since the above expressions apply to a homogeneous gas, and the atmosphere between the observer and each layer is inhomogeneous, Curtis-Godson^{30,31} path-averaged values of Su , α_D , and α_L are used. The line parameters (strengths and air-broadened half-widths) are tabulated in a file generated from the HITRAN atlas¹⁸ that has been supplemented with lines for NO^+ and higher vibrational states of NO and O_3 .

2.5.2 Calculation for Multiple Lines

In the absence of line overlap, the radiances for each line within the spectral bin would sum to form the total radiance and the equivalent widths for each line would sum to form the total equivalent width. The presence of overlap reduces these total quantities. A simple line overlap treatment is used which provides reasonable agreement with exact results for typical atmospheric conditions. The assumption, valid in the statistical limit, is made that the lines are randomly distributed within each bin. Then the combined equivalent width for the total path, W_N , is given by

$$W_N = \Delta\nu \left[1 - \left(1 - \frac{W_{1N}}{\Delta\nu}\right) \left(1 - \frac{W_{2N}}{\Delta\nu}\right) \cdots \left(1 - \frac{W_{kN}}{\Delta\nu}\right) \right] , \quad (14)$$

for " k " lines in the bin. Equation (14) gives the correct equivalent width for the τ calculation (Equation (9)). To compute an approximate overlap-corrected radiance, first the simple radiance sum is taken over all lines in the bin. The result is then multiplied by the ratio of the combined equivalent width from Equation (14) to the equivalent width sum for those lines. A more accurate formulation could be implemented if desired which treats the line overlaps separately in each path segment.

2.5.3 Illustrative Calculations

The accuracy of the LOS radiance algorithm has been explored through comparisons to standard high-resolution LBL calculations for typical atmospheric conditions. A number of different regimes were investigated, including vertical and horizontal viewing geometries, optically thin and thick lines, multiple overlapping lines and bands, and LTE and non-LTE conditions. Below, we discuss representative results for the CO₂ 15 μ m region.

Evaluations of the Curtis-Godson and Rogers-Williams approximations are illustrated by calculations on two individual CO₂ ν_2 lines, one strong (Q10, $\omega_o = 667.494$ cm⁻¹, $S = 3.35 \times 10^{-19}$ cm⁻¹/molec/cm⁻² at 244 K) and one weak (R56, $\omega_o = 713.134$ cm⁻¹, $S = 8.24 \times 10^{-22}$ cm⁻¹/molec/cm⁻² at 244 K). The 1976 US Standard Atmosphere³⁴ was used to define the kinetic temperature and species number densities. The atmosphere is layered into 2 km steps from 51 to 149 km and 10 km steps from 155 to 295 km. We consider two types of multi-segmented paths, zenith views from 60.5 km altitude to 65.5, 71.5, 81.5, and 101.5 km altitudes, and a 60 km limb path. The vertical paths thus have 3, 6, 11, and 21 segments along the LOS while the limb path has 121 segments along the LOS.

The calculated radiance values along with their percent error versus "exact" LBL grid calculations are summarized in Tables 2 and 3. The errors range from 3.4 to 4.9% for the strong line and from 2.0 to 8.7% for the weak line. These errors are consistent with those expected for the equivalent width approximations. The limb calculation with the strong line is a good test since the temperature, pressure, and density vary considerably along the path.

A complete spectrum for the CO₂ ν_2 region is shown in Figure 6 for a 50 km full-limb view. This calculation provides a test of the line overlap treatment, since at this altitude there is significant overlap in the Q branch of the strong 667.380 cm⁻¹ band. The agreement with an "exact" LBL calculation, carried out with FASCOD3, is seen to be excellent over virtually the entire 300 cm⁻¹ spectral range and the six-order-of-magnitude range of radiance. The only major discrepancies are due to the omission in this SHARC version of three weak vibrational bands, which are responsible for the features around 508, 582, and 757 cm⁻¹.

Table 2. Calculated Radiances for Strong Line (Q10) of CO₂ ν_2 .

| <u>FINAL ALTITUDE</u> | <u>RADIANCE (10⁻⁸ W/sr/cm²)</u> | | <u>ERROR (%)</u> |
|---------------------------|---|------|----------------------|
| | SHARC | LBL | |
| 61.5 km | 2.36 | 2.34 | 0.9 |
| 65.5 | 3.25 | 3.11 | 4.5 |
| 71.5 | 3.48 | 3.32 | 4.7 |
| 81.5 | 3.51 | 3.35 | 4.9 |
| 101.5 | 3.51 | 3.35 | 4.9 |
| 60 km Limb | 25.9 | 26.8 | 3.4 |

Table 3. Calculated Radiances for Weak Line (R56) of CO₂ ν_2 .

| <u>FINAL ALTITUDE</u> | <u>RADIANCE (10⁻⁸ W/sr/cm²)</u> | | <u>ERROR (%)</u> |
|---------------------------|---|-------|----------------------|
| | SHARC | LBL | |
| 61.5 km | 0.897 | 0.865 | 3.7 |
| 65.5 | 3.05 | 2.81 | 8.5 |
| 71.5 | 3.54 | 3.25 | 8.7 |
| 81.5 | 3.69 | 3.39 | 8.7 |
| 101.5 | 3.69 | 3.39 | 8.7 |
| 60 km Limb | 16.9 | 17.3 | 2.0 |

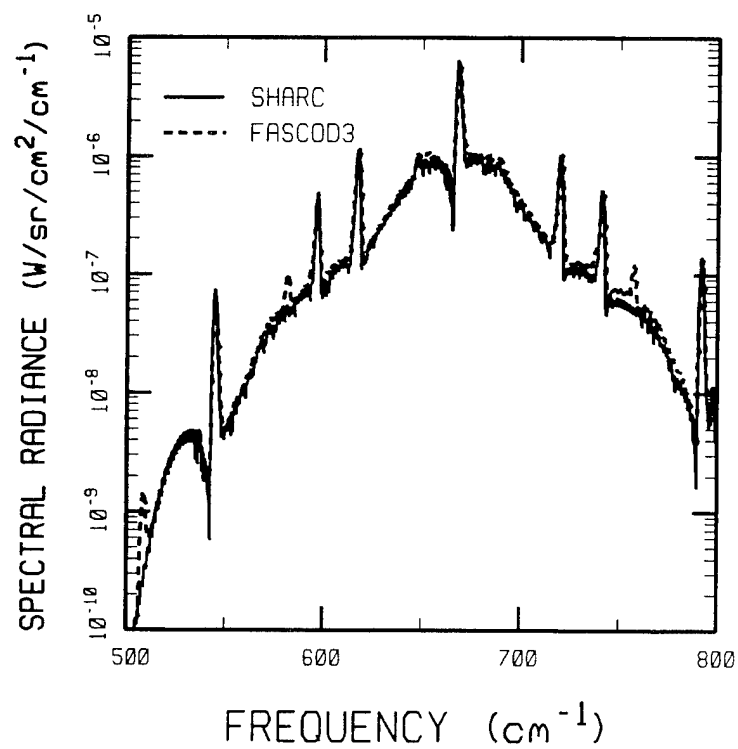


Figure 6. Comparison of SHARC and FASCOD3 Calculations of CO₂ Radiance for a 50 km Limb View.

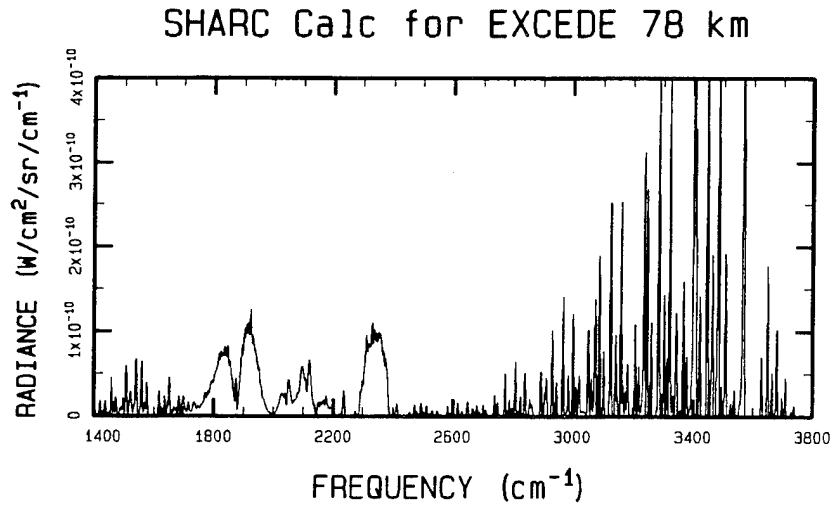
3. DATA COMPARISONS

While comparisons with other computer codes can validate the numerical procedures, comparisons with upper atmospheric IR data are needed to test the physical models in SHARC, including kinetic mechanisms, rate constants, and properties of the atmosphere. A comprehensive validation of these models will require a considerable effort and a very large measurement database. Here, we present illustrative comparisons of predictions and data from several rocket experiments sponsored by the US Air Force/Phillips Laboratory.

Figure 7 shows a predicted emission spectrum from the quiescent nighttime atmosphere in a near-limb view (4° elevation angle) from an altitude of 78 km. The spectral resolution has been degraded to 4 cm^{-1} FWHM. The 1400 to 3800 cm^{-1} region shown contains a varied assortment of molecular emission features, including resolved lines of the $\text{H}_2\text{O } \nu_2$ band (1400 - 1700 cm^{-1}), the $\text{NO } \Delta v=1$ band (1700 - 2000 cm^{-1}), which is emitted from thermospheric altitudes, several $\text{O}_3 \nu_1 + \nu_3$ bands (2000 - 2140 cm^{-1}) generated from chemiluminescent as well as collisional processes, the $\text{CO } \Delta v=1$ band (2100 - 2200 cm^{-1}), the $4.3\text{ }\mu\text{m CO}_2 \nu_3$ feature (2300 - 2400 cm^{-1}), consisting of a number of optically thick, radiatively trapped bands, and resolved $\text{OH } \Delta v=1$ nightglow lines (beyond around 2500 cm^{-1}). All of these emission bands are non-LTE.

The Figure 7a calculation simulates the quiescent atmospheric radiance during the recent EXCEDE III experiment,³⁵ which measured IR emissions induced by dosing the atmosphere with an electron beam. The experiment, flown in April 1990 from White Sands Missile Range, NM, collected both beam-on and beam-off data in a slant-viewing geometry using cryogenically-cooled Michelson interferometers that covered a wide spectral range (around 500 - 5000 cm^{-1}) with high resolution (approximately 2 cm^{-1}). Late in the flight, the sensor rolled towards the horizon, and during a beam-off period near 78 km altitude it obtained data, shown in Figure 7b, in an average viewing geometry similar to that of the SHARC calculation in Figure 7a. All of the features predicted by SHARC appear to be present, and they generally agree very well in both shape and absolute intensity. An exception is the NO band, which is three times stronger than predicted, indicating too low a concentration in the SHARC model atmosphere. This discrepancy is not very disturbing considering the large variability of NO. The good quantitative prediction of the $\text{CO}_2 \nu_3$ feature is quite satisfying, since it presents the most severe test of SHARC's atmospheric excitation and LOS radiation transport algorithms.

a.



b.

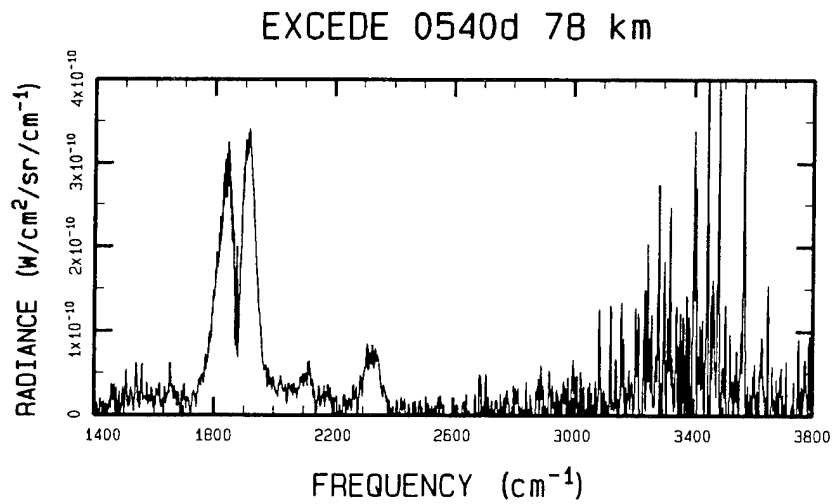


Figure 7. Comparison of SHARC Calculation (Top) and Observation (Bottom) of Quiescent Nighttime Emission in a Near-Limb View from an Altitude of 78 km.

A more detailed examination of the $\text{CO}_2 \nu_3$ feature is provided in Figure 8, which shows limb radiance profiles measured in another experiment, SPIRE,¹⁹ launched from Poker Flat near the dawn terminator. Different phenomena dominate the excitation in various altitude ranges, and this is reflected in the solar angle dependence. During the day, the primary isotope is solar-excited above 110 km, while at lower altitudes the radiance is enhanced by pumping of the $2.7 \mu\text{m}$ band and by emissions from hot bands and minor isotopes. As the density increases, the solar excitations are quenched, and single-quantum excitation of the primary isotope again dominates. The good agreement between the data and the SHARC calculations indicates that these processes are treated accurately.

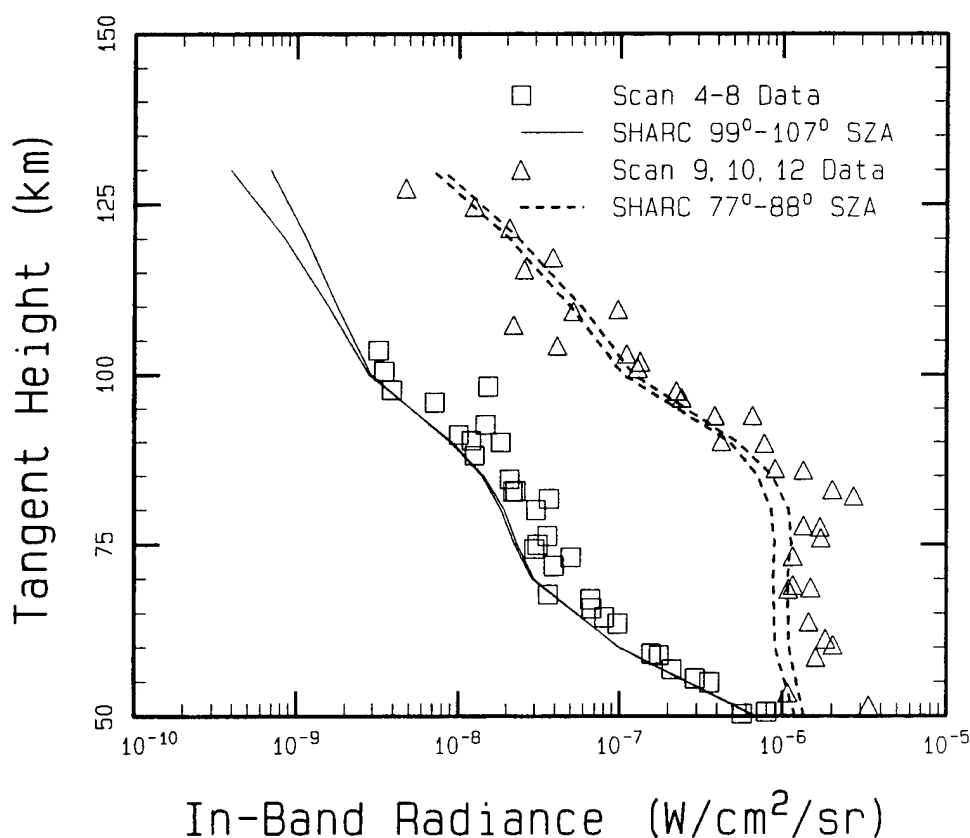


Figure 8. CO_2 4.3 μm Band Limb Radiance Measured in the SPIRE Rocket Experiment and Predicted by SHARC for Different Solar Zenith Angles Near the Dawn Terminator.

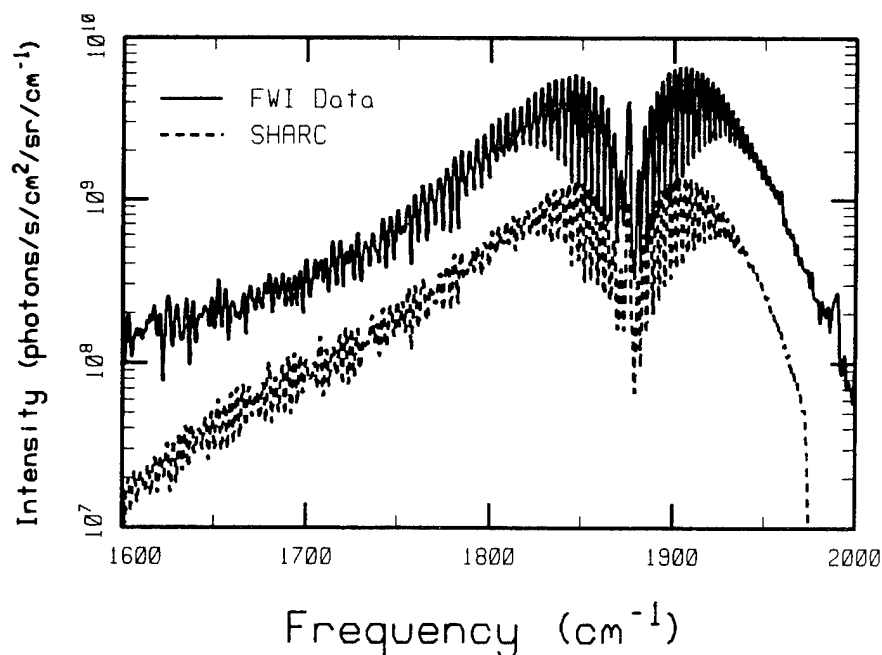


Figure 9. Calculated and Observed NO Spectrum for a 90 km Zenith View During a Class II Aurora.

An example of SHARC's auroral capability is shown in Figure 9. A nitric oxide spectrum from the 1973 Field-Widened Interferometer experiment,³⁶ which observed an IBC Class II aurora, is compared with a SHARC model calculation at a resolution of 1 cm^{-1} . The overall band shape, which includes strong aurorally-induced hot band contributions, is reproduced well by the calculation, except near the edges of the band where non-LTE rotational populations, not currently modeled in SHARC, yield enhanced high-J lines. The overall absolute radiance falls a factor of four below the data; however, the results are quite promising for an *ab initio* calculation that starts with electron dosing of the ambient atmosphere.

Numerous other data/model comparisons have been and are currently being performed for all of the major atmospheric IR emission bands during daytime, nighttime, and auroral conditions. The results will be reported in future papers.

4. CONCLUSIONS

A new, first-principles computer model, SHARC, has been developed by the Air Force for the rapid and accurate calculation of non-LTE upper atmospheric IR radiance and transmittance spectra with a resolution of better than 1 cm^{-1} . SHARC treats the important molecular bands from $2\text{ }\mu\text{m}$ to $40\text{ }\mu\text{m}$ (250 cm^{-1} to $5,000\text{ cm}^{-1}$) for arbitrary lines of sight in the 50-300 km altitude range, accounting for the detailed production, loss, and energy transfer processes among the vibrational states. Calculated vibrational temperatures are very similar to results from other non-LTE codes, and SHARC's equivalent-width spectral algorithm is found to give very good agreement with much more time-consuming "exact" line-by-line methods.

Detailed comparisons of SHARC radiance predictions with field measurements are ongoing. Comparisons performed to date indicate satisfying agreement for most emission bands, including the CO_2 $4.3\text{ }\mu\text{m}$ feature, which poses an especially severe test of the code. Data simulations using SHARC may be valuable in remote sensing of the upper atmosphere, such as for deriving density profiles for variable species such as NO, O_3 , and H_2O .

5. ACKNOWLEDGEMENTS

The authors gratefully acknowledge many useful discussions and comments from Ramesh Sharma, PL/GPOS and Rebecca Healy of Yap Analytics, Inc. during the development and coding of SHARC. The authors also wish to thank Anthony Ratkowski and William Blumberg (PL) for their support during development. This work was funded by the Strategic Defense Initiative Organization under Air Force Contract No. F19628-91-C-0083.

6. REFERENCES

1. F. X. Kneizys, E. P. Shettle, W. O. Gallery, J. H. Chetwynd, Jr., L. W. Abreu, J. E. A. Selby, S. A. Clough, and R. W. Fenn, "Atmospheric Transmittance/Radiance: Computer Code LOWTRAN 6," AFGL-TR-83-0187, Air Force Geophysics Laboratory, Hanscom AFB, MA (1983) ADA137796.
2. A. Berk, L. S. Bernstein, and D. C. Robertson, "MODTRAN: A Moderate Resolution Model for LOWTRAN 7," Spectral Sciences Inc. Rpt. No. SSI-TR-154, Final Report under Contract F19628-86-C-0079; Rpt. No. GL-TR-89-0122, Geophysics Laboratory, Hanscom AFB, MA (1989), ADA214337.
3. S. A. Clough, F. X. Kneizys, E. P. Shettle, and G. P. Anderson, "Atmospheric Radiance and Transmittance: FASCOD2". Proceedings of the Sixth Conference on Atmospheric Radiation, pp. 141-144, American Meteorological Society, Boston, MA (1986).
4. R. D. Sharma, A. J. Ratkowski, R. L. Sundberg, J. W. Duff, L. S. Bernstein, P. K. Acharya, J. H. Gruninger, D. C. Robertson, and R. J. Healey, "Description of SHARC, The Strategic High-Altitude Radiance Code," GL-TR-89-0229, Environmental Research Papers No. 1036, Geophysics Laboratory, Hanscom AFB, MA 01731 (1989) ADA206236.
5. R. D. Sharma, J. W. Duff, R. L. Sundberg, L. S. Bernstein, J. H. Gruninger, D. C. Robertson, and R. J. Healey, "Description of SHARC-2, The Strategic High-Altitude Radiance Code," PL-TR-91-2071, Phillips Laboratory, Hanscom AFB, MA 01731 (1991), ADA239008.
6. R. D. Sharma, J. W. Duff, R. L. Sundberg, J. H. Gruninger, L. S. Bernstein, D. C. Robertson, S. M. Adler-Golden, M. W. Matthew, and R. J. Healey, "User's Manual for SHARC-3, The Strategic High-Altitude Radiance Code," Spectral Sciences, Inc. Rpt. No. SSI-SR-25. Prepared for Phillips Laboratory, Hanscom AFB, MA under Contract No. F19628-91-C-0083 (1993).
7. P. P. Wintersteiner, R. H. Picard, R. D. Sharma, J. R. Winick, and R. A. Joseph, "Line-by-Line Radiative Excitation Model for the Non-Equilibrium Atmosphere: Application to CO₂ 15- μ m Emission," J. Geophys. Res., 97, 18083 (1992).
8. M. Lopez-Puertas, R. Rodrigo, A. Molina, and F. W. Taylor, "A Non-LTE Radiative Transfer Model for Infrared Bands in the Middle Atmosphere, I, Theoretical Basis and Application to CO₂ 15 μ m Bands," J. Atmos. Terr. Phys., 48, 729 (1986).

9. M. Lopez-Puertas, R. Rodrigo, J. J. Lopez-Moreno, and F. W. Taylor, "A Non-LTE Radiative Transfer Model for Infrared Bands in the Middle Atmosphere, II, CO₂ (2.7 and 4.3 μ m) and Water Vapor (6.3 μ m) Bands and N₂(1) and O₂(1) Vibrational Levels," J. Atmos. Terr. Phys., **48**, 749 (1986).
10. To obtain the SHARC code, contact Dr. R. D. Sharma, PL/GPOS, 29 Randolph Road, Hanscom AFB, MA 01731-5000.
11. L. S. Bernstein, "Non-Equilibrium Molecular Emission and Scattering Intensity Subroutine (NEMESIS)," Spectral Sciences Inc. Rpt. No. SSI-TR-136 under Contract F19628-87-C-0130; AFGL-TR-88-0124, Air Force Geophysics Laboratory, Hanscom AFB, MA (1988) ADA199295.
12. D. C. Robertson, P. K. Acharya, S. M. Adler-Golden, L. S. Bernstein, F. Bien, J. W. Duff, J. H. Gruninger, R. L. Sundberg, R. J. Healey, J. M. Sindoni, P. M. Bakshi, A. Dalgarno, and B. Zygelman, "Investigations into Atmospheric Radiative Processes in the 50-300 km Regime," Spectral Sciences Inc. Rpt. No. SSI-TR-188, Final Report under Contract F19628-87-C-0130; PL-TR-91-2137, Phillips Laboratory, Hanscom AFB, MA (1991), ADA251588.
13. R. J. Kee, J. A. Miller, and T. H. Jefferson, "CHEMKIN: Problem-Independent, Transportable, Fortran Chemical Kinetics Code Package," Sandia Rpt. No. SAND80-8003, Sandia National Laboratory, Livermore, CA 94550 (1980).
14. J. B. Kumer and T. C. James, "CO₂ (001) and N₂ Vibrational Temperatures in the $50 \leq Z \leq 130$ km Altitude Range," J. Geophys. Res., **79**, 638 (1974).
15. J. B. Kumer, "Atmospheric CO₂ and N₂ Vibrational Temperatures at 40- to 140-km Altitude," J. Geophys. Res., **82**, 16 (1977).
16. J. B. Kumer, A. T. Stair, Jr., N. Wheeler, K. D. Baker, and D. J. Baker, "Evidence for an OH \dagger \rightarrow N₂ \dagger \rightarrow CO₂(ν_3) \rightarrow CO₂+h ν (4.3 μ m) Mechanism for 4.3- μ m Airglow," J. Geophys. Res., **83**, 4743 (1978).
17. R. L. Taylor, "Energy Transfer Processes in the Stratosphere," Can. J. Chem., **52**, 1436 (1974).
18. L. S. Rothman, R. R. Gamache, A. Goldman, L. R. Brown, R. A. Toth, H. M. Pickett, R. L. Poynter, J. M. Flaud, C. Camy-Peyret, A. Barbe, N. Husson, C. P. Rinsland, and M. A. H. Smith, "The HITRAN Database: 1986 Edition," Appl. Optics, **26**, 4058 (1987).
19. A. T. Stair, Jr., R. D. Sharma, R. M. Nadile, D. J. Baker, and W. F. Grieder, "Observations of Limb Radiance with Cryogenic Spectral Infrared Rocket Experiment," J. Geophys. Res., **90**, 9763 (1985).
20. A. E. Hedin, "Extension of the MSIS Thermosphere Model Into the Middle and Lower Atmosphere," J. Geophys. Res., **96**, 1159 (1991).

21. C. P. Rinsland, M. R. Gunson, R. Zander, and M. Lopez-Puertas, "Middle and Upper Atmosphere Pressure-Temperature Profiles and the Abundances of CO₂ and CO in the Upper Atmosphere From ATMOS/Spacelab 3 Observations," J. Geophys. Res., 97, 20479 (1992).
22. (a) P. P. Wintersteiner, R. A. Joseph, and A. J. Paboojian, "High-Altitude Non-Equilibrium Infrared Emission Models," ARCON Corporation, Final Report under Contract F19628-86-C-0118; GL-TR-90-0311, Geophysics Laboratory, Hanscom AFB, MA (1990), ADA232503.
 (b) H. Nebel, R. D. Sharma, P. P. Wintersteiner, and R. A. Joseph, "CO₂ (4.3 μ m) Vibrational Temperatures and Limb Radiances under Sunlit Conditions in the 50-120 km Altitude Range," EOS, Proceedings of the American Geophys. Union, Fall 1989, San Francisco, CA.
23. M. Lopez-Pertas, M. A. Lopez-Valverde, C. P. Rinsland, and M. R. Gunson, "Analysis of the Upper Atmosphere CO₂(ν_2) Vibrational Temperatures Retrieved From ATMOS/Spacelab 3 Observations," J. Geophys. Res., 97, 20469 (1992).
24. A. E. Grün, "Luminescenz-photometrische Messungen der Energieabsorption im Strahlungsfeld von Elektronenquellen Eindimensionaler Fall im Luft," Z. Naturforsch., 112a, 89-95 (1957).
25. M. H. Rees, "Auroral Ionization and Excitation by Incident Energetic Electrons," Planet. Space Sci., 111, 1209-18 (1964).
26. D. J. Strickland, J. R. Jasperse, and J. A. Whalen, "Dependence of Auroral FUV Emissions on the Incident Electron Spectrum and Neutral Atmosphere," J. Geophys. Res., 88, 8051-62 (1983).
27. J. P. Winick, R. H. Picard, R. A. Joseph, R. D. Sharma, and P. P. Wintersteiner, "AARC: The Auroral Atmospheric Radiance Code," AFGL-TR-87-0334, Air Force Geophysics Laboratory, Hanscom AFB, MA 01731 (1987) ADA202432.
28. O. Ashihara and K. Takayanagi, "Velocity Distribution of Ionospheric Low-Energy Electrons," Planet. Space Sci., 22, 1201 (1974).
29. J. B. Kumer, "Theory of the CO₂ 4.3 μ m Aurora and Related Phenomena," J. Geophys. Res., 82, 2203 (1977).
30. A. R. Curtis, "A Statistical Model for Water Vapour Absorption," Q. J. R. Meteorol. Soc., 78, 638-640 (1952)
31. W. L. Godson, "The Evaluation of Infrared-Radiative Fluxes due to Atmospheric Water Vapour," Q. J. R. Meteorol. Soc., 79, 367-379 (1953).
32. C. B. Ludwig, W. Malkmus, J. E. Reardon, and J. A. Thomson, Handbook of Infrared Radiation From Combustion Gases, Rpt. No. SP-3080, Scientific and Technical Information Office, NASA, Washington, DC (1973).

33. C. D. Rodgers and A. P. Williams, "Integrated Absorption of a Spectral Line with the Voigt Profile," J. Quant. Spectrosc. Radiat. Transfer, 14, 319 (1974).
34. "U. S. Standard Atmosphere 1976," National Oceanic and Atmospheric Administration, NOAA-S/T 76-1562, U.S. Govt. Printing Office, Washington DC (1976).
35. R. E. Murphy, "EXCEDE III Catalog of Corrected Spectra and Corrected Interferograms," Rpt. Nos. 12-15, Research Sciences Corp., Lexington, MA (1992-3).
36. P. J. Espy, C. R. Harris, A. J. Steed, J. C. Ulwick, R. H. Haycock, and R. A. Straka, "Rocketborne Interferometer Measurement of Infrared Auroral Spectra," Planet. Space Sci., 36, 543 (1988).